communications biology

A Nature Portfolio journal

Article

https://doi.org/10.1038/s42003-025-07824-3

Protein disulfide isomerase is essential for osteoblast differentiation in mice

Check for updates

Yue Lu[1] ✉, Aizhen Yang[1], Zhenzhen Zhao[1], Yue Han[2], Depei Wu[2] ✉ & Yi Wu[1] ✉

Protein disulfide isomerase (PDI) is an oxidoreductase responsible for the formation, reduction and isomerization of disulfide bonds of nascent proteins in endoplasmic reticulum (ER). So far, the role of PDI in bone biology has never been characterized using genetically-modified animal models. In this study we generated osteoblast- specific PDI-deficient mice by crossing PDI-floxed ($PDI^{fl/fl}$) mice with Osx-Cre mice. Compared with their littermate control $PDI^{fl/fl}$ mice, homozygous osteoblast-knockout mice (Osx-Cre/$PDI^{fl/fl}$) were embryonically lethal, but heterozygous knockout mice (Osx-Cre/$PDI^{fl/wt}$) displayed significantly pronounced growth retardation and reduced bone length. Besides, the decreases in bone density, osteoblast and osteoclast numbers, collagen fiber content and bone formation rate were observed in Osx-Cre/$PDI^{fl/wt}$ mice. Osteoblast precursors isolated from $PDI^{fl/fl}$ mice were infected with Cre recombinant adenovirus to produce PDI-deficient osteoblasts, followed by induction of differentiation. Osteoblasts deficient of PDI had decreased alkaline phosphatase activity, mineralizing capacity, and differentiation. Quantitative protein mass spectrometry analysis and immunoblotting showed that PDI deficiency markedly decreased the expression of the α-subunits of collagen prolyl 4-hydroxylase (C-P4H), including P4HA1, P4HA2 and P4HA3. These results demonstrate that PDI plays an essential role in osteoblast differentiation and bone formation and is required for the expression of the α-subunit of C-P4H in osteoblasts.

As bone-forming cells, osteoblasts contain a large amount of endoplasmic reticulum (ER) within the cytoplasm, which are crucial for the synthesis and processing of large quantities of the proteins necessary for bone formation like collagen. Protein disulfide isomerases (PDIs) family are a group of thiol oxidoreductases localized in ER[1]. This family contains 21 members in mammals[2]. PDI, which is encoded by *P4HB* gene, is a prototypical member of the PDI family. It consists of four thioredoxin-like domains a, b, a' and b'. Both the a and a' domains have the CGHC catalytic motif, while the b and b' domains lack this active motif and are mainly responsible for the binding of the substrates[3–7]. PDI is widely involved in the processes of various pathological conditions such as diabetes, cardiovascular disease, cancer, and neurodegenerative disorders[8–11]. A previous study has shown that ERp57, which is one of the PDI family member, participates in osteoblast formation[12], suggesting that the PDI family play a role in osteoblast biology. Mutations in the PDI gene *P4HB* located on chromosome 17 (17q25.3)[13] are associated with Cole-Carpenter syndrome, which is a severe subtype of osteogenesis imperfecta, distinguished by bone fragility, skull defects, exophthalmos, hydrocephalus, and distinctive facial features[13–16]. Moreover, downregulation of PDI is associated with low bone intensity in patients with osteoporosis[17]. Although these studies suggest that PDI is involved in in bone biology, its role has never been characterized by genetically modified model, and the function of this gene and the underlying mechanisms remain elusive[13,14,18–23].

In this study, using an osteoblasts-specific *P4HB* (PDI)-knockout mouse model, we investigated the role of PDI in bone development. We found that downregulated PDI expression in osteoblasts decreased bone length and density, and impaired growth plate development. Additionally, PDI deficiency caused a reduction of osteoblast numbers, osteoblast ER stress, and a decrease in expression of collagen proline 4-hydroxylase alpha subunits. Thus, this study provides the genetic evidence demonstrating that PDI is essential for osteoblast differentiation.

Results

Deletion of PDI in osteoblasts inhibits bone growth

Our previous studies demonstrated that whole-body knockout of PDI resulted in embryonic lethality[24]. To overcome this limitation and

[1]Cyrus Tang Medical Institute, Collaborative Innovation Center of Hematology, State Key Laboratory of Radiation Medicine and Prevention, Soochow University, Suzhou, 215123, China. [2]National Clinical Research Center for Hematologic Diseases, Jiangsu Institute of Hematology, Institute of Blood and Marrow Transplantation, Collaborative Innovation Center of Hematology, First Affiliated Hospital of Soochow University, Suzhou, 215006, China.
✉e-mail: luyue22215@163.com; wudepei@suda.edu.cn; wuy@suda.edu.cn

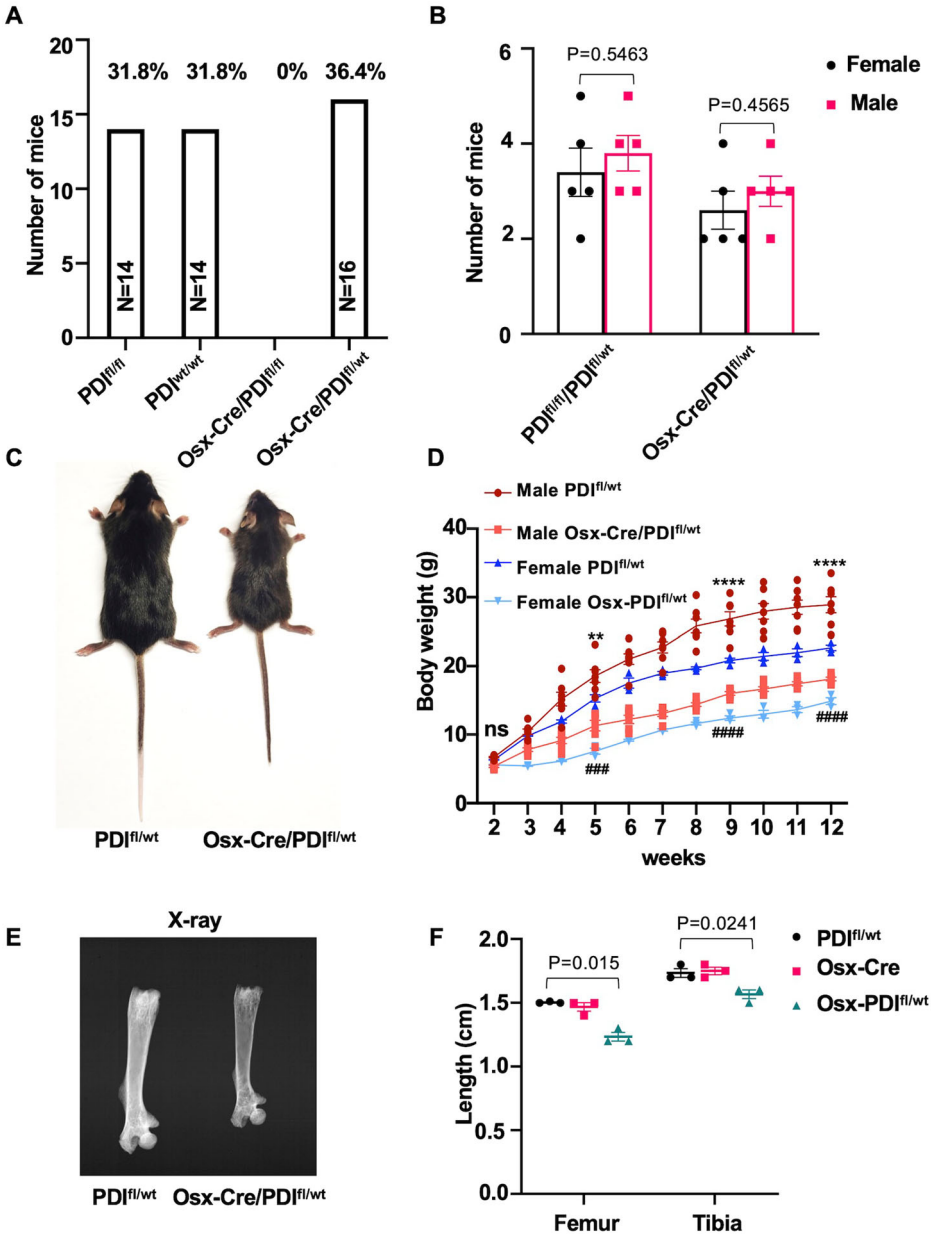

Fig. 1 | Conditional PDI knockout in Osx-Cre/PDI$^{fl/wt}$ mice results in impaired bone growth. **A** Genotype analysis of offspring from matings between Osx-Cre/PDI$^{fl/wt}$ and control (PDI$^{fl/fl}$) mice. Genotypes were identified using PCR, and the distribution percentages of each genotype were calculated and displayed based on the analysis results. **B** Sex ratio (male-to-female) analysis of offspring, with no significant differences between groups (n = 5). **C** Representative images of 8-week-old Osx-Cre/PDI$^{fl/wt}$ and control (PDI$^{fl/wt}$) mice. Osx-Cre/PDI$^{fl/wt}$ mice are visibly smaller than their littermate controls. **D** Growth curves demonstrate significant growth retardation in Osx-Cre/PDI$^{fl/wt}$ mice beginning at 2 weeks of age. Significant differences in growth are indicated for males (*) and females (#). Data are presented as Mean ± SEM, n = 3–7. **P < 0.01, ****P < 0.0001 for males; ###P < 0.001, ####P < 0.0001 for females. **E** Femurs were collected from 8-week-old male Osx-Cre/PDI$^{fl/wt}$ mice and control (PDI$^{fl/wt}$) mice, followed by X-ray imaging. **F** Femurs and tibias were collected from 8-week-old Osx-Cre/PDI$^{fl/wt}$ mice and control mice, followed by quantitative analysis of bone length using high-precision digital measurement instruments (n = 3). Two-tailed t test for two groups and One-way ANOVA followed by a Dunn's multiple comparison for multiple groups were used. Data are presented as mean ± SEM. Source data are provided in Supplementary Data.

investigate the specific role of PDI in bone biology, we employed the Cre/loxP recombination system. Osteoblasts are critical bone-forming cells. To determine the role of PDI in osteoblasts, PDI$^{fl/fl}$ mice were crossed with Osx-Cre mice to generate osteoblast-specific PDI knockout mice (Supplementary Fig. 1A-B). The distribution of the offsprings from the 10 litters showed no homozygous osteoblast PDI-knockout (Osx-Cre/PDI$^{fl/fl}$) mice were produced (Fig. 1A), indicating that the homozygous deletion of osteoblast *P4HB* is lethal. To assess knockout efficiency, both mRNA and protein levels of PDI were measured. PDI mRNA expression in the cortical bone of Osx-Cre/PDI$^{fl/wt}$ mice was significantly reduced compared to PDI$^{fl/fl}$ control mice (Supplementary Fig. 1C). Additionally, quantification of PDI expression in the growth plates of E18.5 mice showed a marked reduction in Osx-Cre/PDI$^{fl/fl}$ mice relative to the PDI$^{fl/fl}$ controls (Supplementary Fig. 1D-E), thus indicating the successful targeting of PDI. There was no significant difference in the male- to- female ratio of the Osx-Cre/PDI$^{fl/wt}$ mice offsprings (Fig. 1B). Compared with littermate control PDI$^{fl/fl}$ mice, Osx-Cre/PDI$^{fl/wt}$ mice had a significantly smaller body size (Fig. 1C). Besides, both male and female Osx-Cre/PDI$^{fl/wt}$ mice presented slower body weight gain than the control mice did from 3 weeks of age (Fig. 1D). As shown by X-ray, Osx-Cre/PDI$^{fl/wt}$ mice had significantly shorter femurs and tibias and reduced bone density compared with the control PDI$^{fl/fl}$ mice (Fig. 1E, F), indicating that osteoblast PDI plays a critical role in growth and development.

Bone volume and bone formation rate are significantly decreased in Osx-Cre/PDI$^{fl/wt}$ mice

To further evaluate the role of PDI in bone formation, eight-week-old male Osx-Cre/PDI$^{fl/wt}$ mice were studied using microcomputed tomography. The femurs of Osx-Cre/PDI$^{fl/wt}$ mice were scanned along with those of wild-type mice, and the bone structures were reconstructed in 3D system. Compared with Osx-Cre mice, Osx-Cre/PDI$^{fl/wt}$ mice had significantly reduced trabecular bone volume and increased trabecular spacing (Fig. 2A, B). To further evaluate the impact of PDI deficiency on bone formation rate, dynamic histomorphometric analysis was performed on 3-week-old mice, sequentially labeled with calcein. Femoral hard tissue sections were prepared, and the distance between two consecutive labels on the femur was measured using fluorescence microscopy to calculate the mineral apposition rate (MAR). Compared with that in control mice, the distance between the labels

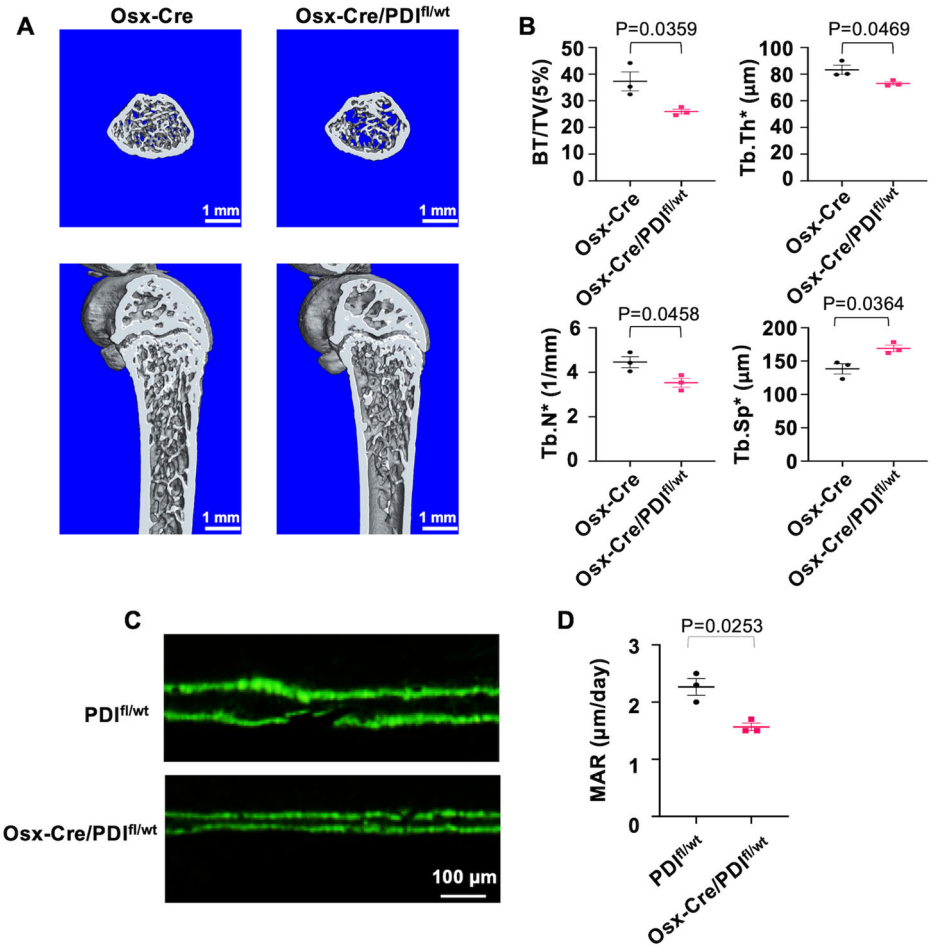

Fig. 2 | Analysis of bone volume and formation rate in Osx-Cre/PDIfl/wt mice. A Femurs from 8-week-old Osx-Cre/PDI$^{fl/wt}$ and Osx-Cre control mice were subjected to micro-CT scanning. Both cross-sectional and longitudinal images were acquired to assess trabecular. **B** Quantitative data of micro-CT results in A. Tb.N*: trabecular number; Tb.Th*: Trabecular Thickness; BV/TV: Bone Volume/Total Volume;Tb.Sp*: Trabecular Space (n = 3). **C**, **D** Calcein double labeling was performed on 3-week-old mice to evaluate dynamic bone formation. Mice received intraperitoneal injections of calcein (10 mg/kg) on days 1 and 5 before euthanasia. Cortical bone sections were analyzed using fluorescence microscopy to measure mineral apposition rates (MAR), which were calculated as the distance between the two calcein labels divided by the time interval (n = 3). Two-tailed Student's t test were used. Data are presented as mean ± SEM. Source data are provided in Supplementary Data.

in osteogenesis-specific PDI-downregulated mice was significantly shorter, indicating that the decreased PDI expression inhibits bone formation rate (Fig. 2C, D). Compared with PDI$^{fl/wt}$ mice, Osx-Cre/PDI$^{fl/wt}$ mice had decreased serum levels of ALP, calcium and phosphorus (Supplementary Fig. 2).

Adipocyte differentiation is promoted in PDI-deficient osteoblasts

Osteoblasts and adipocytes share a common precursor, exhibiting plasticity between these cell types. To determine whether PDI plays a role in the differentiation of osteoblasts and adipocytes, H&E staining was performed on the femurs of 8-week-old male mice. More fatty infiltration was observed in the bone marrow of Osx-Cre/PDI$^{fl/wt}$ mice than that of the control mice (Fig. 3A), suggesting that PDI is involved in the differentiation of osteoblasts and adipocytes. To validate this hypothesis, frozen sections of 8-week-old mice femurs were prepared and stained with oil red, which readily dissolves in lipids and can be used to characterize adipocytes. The number of adipocytes within the bone marrow cavity was significantly increased in mice, with the red portions in the figure representing oil red-stained adipocytes (Fig. 3B, C). Since the homozygous osteoblast-specific PDI-knockout mice did not survive, to further determine the role of PDI in osteoblast differentiation, calvarial cells were isolated from PDI$^{fl/fl}$ and Osx-Cre/PDI$^{fl/wt}$ mice, followed by infection with Ad-Cre and Ad-GFP and induction for 7 days. RNA was extracted from the differentiated cells, and the expression levels of PPARγ, C/EBPα, Fabp4, Adipoq, and Plin1 that are related to adipocyte differentiation, were assessed. The primary PDI deficiency increased the expression levels of these genes following the induced differentiation (Fig. 3D), suggesting that PDI inhibits adipocyte differentiation by downregulating these gene expressions.

PDI downregulation decreases collagen content in bone

Since the toughness of bone largely derives from its organic phase[25], we investigated the underlying mechanism by which PDI regulates bone development, particularly in relation to collagen content and structure. First, paraffin-embedded sections of femurs from 8-week-old mice were stained with picrosirius red (PSR) and visualized using bright-field and polarized light (Fig. 4A, B). Quantification of both imaging modalities revealed similar alterations in collagen structure and organization. Collagen fibril thickness in PSR-stained slides was used to determine color thresholds, revealing a significant increase in the percentage of thin (green) fibrils in bones from Osx-Cre/PDI$^{fl/wt}$ mice compared to the control mice (Fig. 4C). This increase in thinner fibrils was at the expense of thick (red) fibrils, which were significantly decreased in Osx-Cre/PDI$^{fl/fl}$ mice compared to control mice (Fig. 4C), accompanied with significantly lower total amount of collagen fiber bundles (sum of color spectrums) (Fig. 4D). These observations suggest that PDI is necessary for collagen synthesis during bone development.

Homozygous PDI deficiency destroys growth plate structure, inhibits endochondral and intramembranous bone ossification, and reduces osteoclast numbers

Inactivation of PDI in Sp7-expressing cells leads to severe dysplasia, skeletal abnormalities, and lethality at birth. Although Osx-Cre/PDI$^{fl/wt}$ mice exhibit stunted growth, short stature, and short limbs during development, the phenotypes of PDI osteoblast-specific homozygous knockout mice (Osx-Cre/PDI$^{fl/fl}$) are not clear. Thus, Osx-Cre/PDI$^{fl/fl}$ embryos at E18.5 were collected to further determine the role of PDI in bone development. First, Alizarin red and Alcian blue staining showed that E18.5 Osx-Cre/PDI$^{fl/fl}$ embryos were severely underdeveloped (Fig. 5A). Osx-Cre/PDI$^{fl/fl}$ mice had shortened limbs, decreased bone ossification, and disproportionate effects on skull-calvaria, sternum and vertebrae (Fig. 5A). These results suggest that

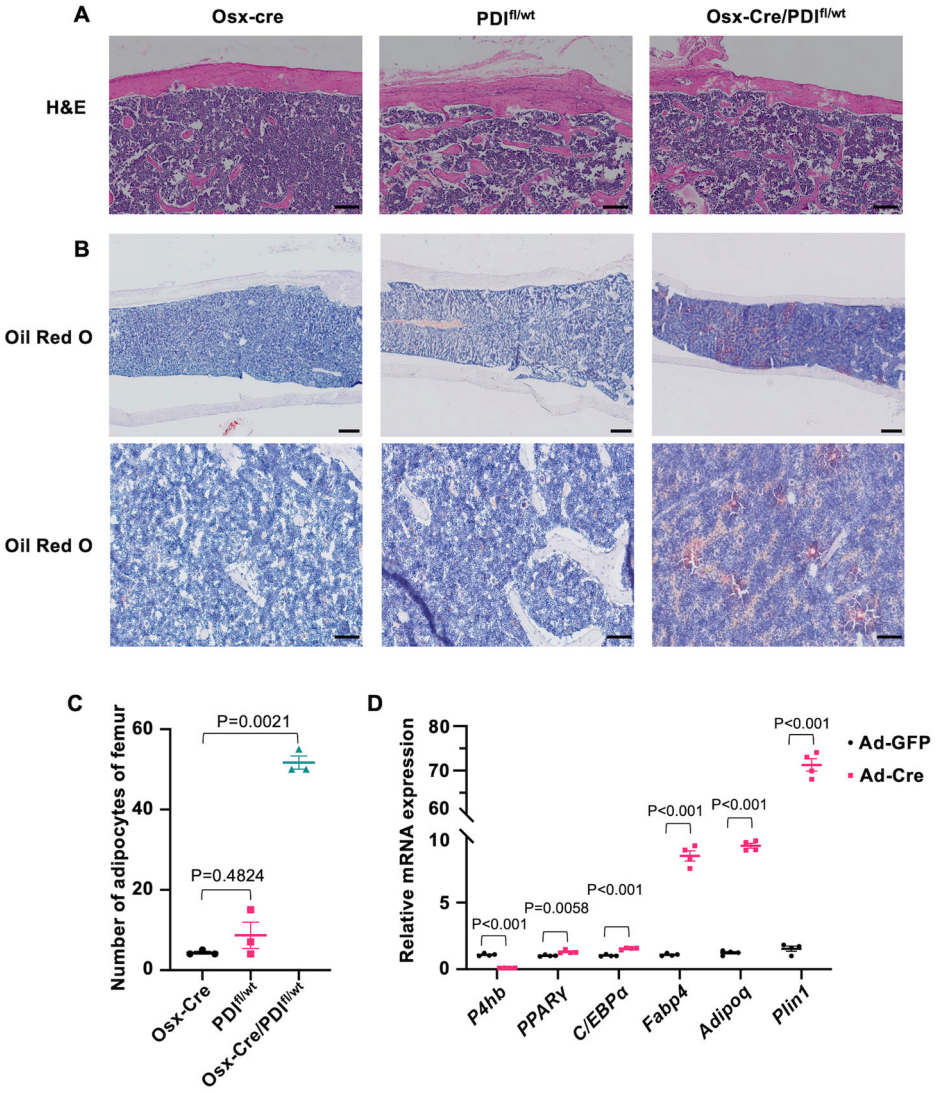

Fig. 3 | Adipocyte differentiation is promoted in PDI deficient osteoblasts. Femurs from 8-week-old Osx-Cre, PDI$^{fl/wt}$, and Osx-Cre/PDI$^{fl/wt}$ mice were harvested and processed for histological analysis. **A**, **B** Hematoxylin and eosin (H&E) and Oil Red O staining were performed to visualize and quantify adipocytes within the bone marrow. H&E staining was used for general tissue morphology, with scale bars = 200 μm. For Oil Red O staining in (**B**), scale bars = 400 μm (top) and 100 μm (bottom) to assess lipid content within the bone marrow. The arrows indicate adipocytes. **C** The number of adipocytes in the entire femur was quantified following Oil Red O staining. Adipocytes were counted in multiple fields of view per section, and the average number was calculated for each group (n = 3). **D** The expression of adipogenic transcription factors and marker genes, including PPARγ, C/EBPα, Fabp4, Adipoq, and Plin1, was evaluated by quantitative qPCR. RNA was extracted from osteoblasts induced by osteogenic medium in Ad-GFP and Ad-Cre infected cells after 7 days of culture. Gene expression levels were normalized to β-actin and compared between groups (n = 4). Two-tailed t test for two groups and One-way ANOVA followed by a Dunn's multiple comparison for multiple groups were used. Data are presented as mean ± SEM. Source data are provided in Supplementary Data.

PDI is critical for maintenance of bone development and bone density. Further, the potential impact of osteoblast PDI deficiency on osteoclast formation was investigated using staining of E18.5 tibia paraffin sections with artrate-resistant acid phosphatase (TRAP) and Von kossa. TRAP staining revealed a significant decrease in the number of osteoclasts in Osx-Cre/PDI$^{fl/wt}$ and Osx-Cre/PDI$^{fl/fl}$ mice compared with the control mice (Fig. 5B). Von Kossa staining revealed decreased osteoblast mineralization and a significantly shorter medullary cavity in Osx-Cre/PDI$^{fl/lwt}$ and Osx-Cre/PDI$^{fl/lfl}$ mice compared with the Osx-Cre and control mice (Fig. 5C). These data suggest that PDI indirectly regulates osteoclast development through its modulation of osteoblasts leading to an imbalance in bone homeostasis and decreased bone density. Besides, as shown by H&E staining, compared with the control mice, Osx-Cre/PDI$^{fl/fl}$ embryos presented shortened and disordered growth plates, a decrease in the length of the resting zone by 20%, a reduction in the length of the proliferation zone by 70%, and a decrease in the length of the hypertrophic zone by 30% (Fig. 6A–F). These findings suggest that the deficiency of PDI in osteoblasts indeed decreases the growth plate development and chondrocyte proliferation impairing longitudinal bone growth, which is probably associated with the embryonic lethality.

PDI deficiency inhibits osteoblast function and differentiation

To further confirm the specific role of PDI in osteoblast differentiation and maturation, primary osteoblast precursors were isolated from the calvaria of neonatal PDI$^{fl/fl}$ mice and infected with adenoviruses expressing Cre (Ad-GFP/Ad-Cre) to induce homozygous knockout of PDI, followed by induction of differentiation to osteoblasts.

As shown in Fig. 7A, infection of Cre virus decreased osteoblast number. ALP and Alizarin Red S staining showed a significant reduction in alkaline phosphatase activity and mineralized nodules upon PDI deletion (Fig. 7B). Cells were collected 72 h after infection and induction, and analyzed by western blotting, which confirmed that PDI was completely deleted in Ad-Cre-infected osteoblasts (Fig. 7C, D). Moreover, as detected by qPCR, the expressions of important osteoblast differentiation marker genes Col1a, ALPL, ATF4, BGLAP, and IBSP got decreased in the PDI-deficient osteoblasts than in the control cells, (Fig. 7E). The OPG content was elevated in the supernatant of Ad-Cre virus-infected PDI$^{fl/fl}$ osteoblast medium, while RANKL content remained unchanged (Fig. 7F). These data demonstrate that PDI is indeed important for osteoblast function and differentiation.

The absence of PDI in osteoblasts results in cell apoptosis and ER stress

To further explore the mechanism underlying the role of PDI in osteoblast biology, the association of PDI deficiency with primary osteoblast apoptosis was analyzed. The expression of apoptosis marker caspase 3 was up-regulated in PDI-deficient osteoblasts (Fig. 8A, B), which was consistent with an increased apoptosis in femoral cells of Osx-Cre/PDI$^{fl/fl}$ mice, as shown by the TUNEL immunofluorescence analysis (Supplementary

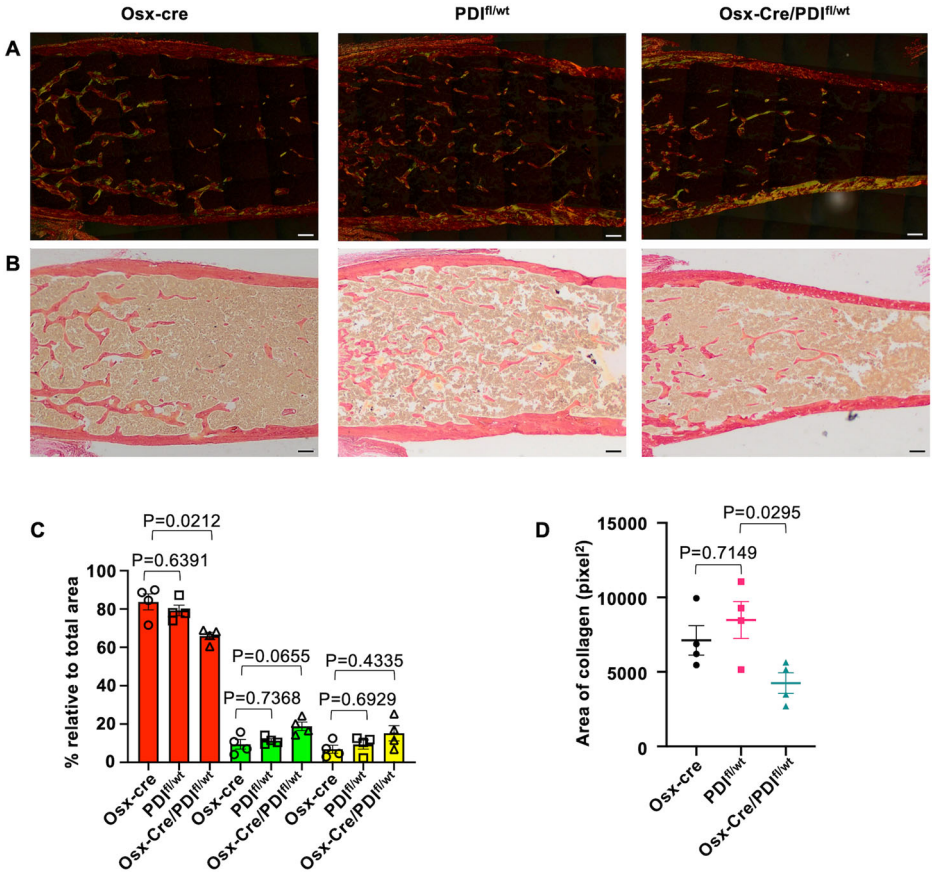

Fig. 4 | Effects of PDI on bone collagen content and organization. Femur sections from 8-week-old mice were stained with Picrosirius Red, with a section thickness of 5 μm. After fixation, dehydration, and paraffin embedding, the samples were observed under polarized light and conventional light. **A** Femur sections from 8-week-old mice were stained with Picrosirius Red and observed under conventional light. **B** The same sections observed under polarized light. Green birefringence under polarized light indicates thin collagen fibers, while yellow and red indicate thick fibers. **C** The birefringence intensity for each color was quantified using Fiji image analysis software to assess the relative proportions of thin and thick collagen fibers (n = 4). **D** The total area of collagen fibers (in pixels²) was calculated (n = 4). Scale bars = 200 μm. One-way ANOVA followed by a Dunn's multiple comparison for multiple groups was used. Data are presented as mean ± SEM. Source data are provided in Supplementary Data.

Fig. 1F-G). Moreover, the expression of ER stress markers was significantly increased in PDI-deficient osteoblasts (Fig. 8A, B). The MTT assay indicated that the absence of PDI had no effect on osteoblast proliferation (Fig. 8D). PDI shares a similar structure and function with other members of the PDI family, such as ERp5, ERp57, and ERp72. As detected by immunoblotting, the expression of ERp5 and ERp57 was increased in PDI-deficient osteoblasts (Fig. 8A), suggesting that PDI deficiency induces the upregulation of ERp5 and ERp57 expression as a compensatory mechanism. Similarly, qPCR results revealed that PDI-deficient osteoblasts exhibited significantly higher expression levels of ERp5, ERp57, and ERp72 than the control cells (Fig. 8C).

PDI deficiency reduces the expression of collagen prolyl 4-hydroxylases (C-P4Hs) α subunits in osteoblasts

To determine the substrates of PDI in osteoblast development, PDI-deficient osteoblasts were evaluated by quantitative mass spectrometry. The results showed a significant down-regulated expression of the α-subunits of collagen prolyl 4-hydroxylase (C-P4H), including P4HA1, P4HA2, and P4HA3, which was confirmed by western blotting (Fig. 9A–C). Decreased P4HA1-3 was probably associated with the poor osteoblast differentiation or osteoblast numbers.

Discussion

In this study, we generated a new mouse strain with specific deletion of PDI expression in osteoblasts and performed a comprehensive analysis of its phenotypes in bone mineral density, bone histomorphology, osteoblast function, and molecular regulatory mechanisms. We found that homozygous osteoblastic deficiency (Osx-Cre/PDI$^{fl/fl}$) was embryonically lethal, and heterozygous Osx-Cre/PDI$^{fl/wt}$ mice exhibited significantly slower growth, shorter body size, and less bone ossification. The homozygous deletion of PDI in isolated osteoblasts results in cellular apoptosis and ER stress, and the downregulation of P4HA1, P4HA2, and P4HA3 expression, which is consistent with the decreased collagen content in the bone. Our data provide the genetic evidence that PDI is essential for osteoblast differentiation, function and collagen formation and is required for the expression of P4Hα subunits.

Bone formation encompasses both endochondral ossification and intramembranous ossification, which are driven by osteoblasts. Osteoblasts originate from mesenchymal stem cells (MSCs), which can differentiate into osteoblasts, chondrocytes, or adipocytes[26]. Osteoblast differentiation is characterized by three distinct stages: proliferation, matrix maturation, and mineralization. Our data indicate that PDI is a critical factor driving osteoblast differentiation. The differentiation of mesenchymal stem cells is primarily regulated by transcription factors, cytokines, hormones, and growth factors[27–29]. Our findings point out the necessity of determining the substrates by which PDI regulates for the differentiation of osteoblasts. The expression of P4HA1, P4HA2 and P4HA3 was significantly decreased in osteoblasts lacking PDI, leading to reduction of collagen formation and the inhibition of the differentiation and function of osteoblasts. Thus, PDI is essential for the expression of the alpha subunits of C-P4H in osteoblasts. Osteoblasts synthesize proteins, including ALP, osteocalcin, and type I collagen[30]. Type I collagen constitutes more than 90% of the organic material in bone tissue[31]. Most cases of osteogenesis imperfecta cases are characterized by abnormalities in type I collagen. While impaired formation of type I collagen was not observed in skin fibroblasts from patients with Cole-Carpenter syndrome, a significant decrease in collagen fiber content was detected in the femurs of Osx-Cre/PDI$^{fl/wt}$ mice, suggesting that PDI plays a more prominent role in collagen formation within osteoblasts than in skin fibroblasts do. As a subunit of C-P4H, PDI can catalyze the formation of 4-hydroxyproline on collagen, enabling collagen to form a stable triple helix structure. There are three isozymes of collagen proline 4-hydroxylase (C-P4H-I, C-P4H-II, and C-P4H-III), which differ in their α subunits but all have a PDI β subunit, forming an α2β2 tetramer. The role of PDI as the β-subunit of C-P4H enzyme is to enable the insoluble α-subunit to form a

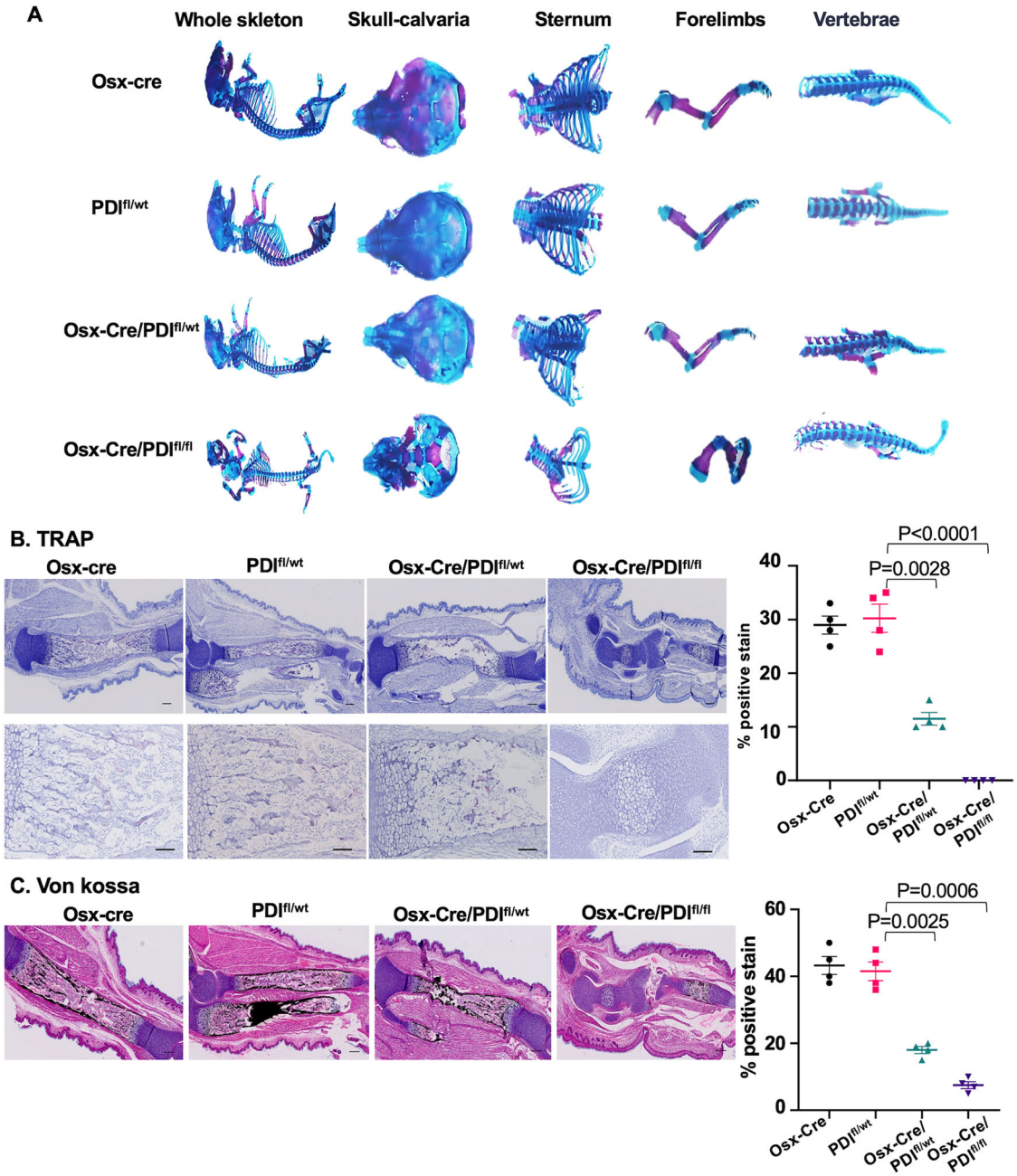

Fig. 5 | Assessment of endochondral bone ossification in homozygous Osx-Cre/PDIfl/fl mice at E18.5. A Whole-mount skeletal staining using Alizarin red and Alcian blue was conducted on E18.5 mice. Osx-Cre/PDI$^{fl/fl}$ mice exhibit shortened limbs, reduced bone ossification, and disproportionately affected skull-calvaria, sternum and vertebrae. Tibias were dissected, fixed in 10% formalin, decalcified, and embedded in paraffin. Sections were cut at 5 μm thickness and stained with (**B**) TRAP to evaluate osteoclast activity and (**C**) Von Kossa (uncalcified bone tissues) to assess mineralization of the bone matrix. Scale bars = 100 μm. Histomorphometric analysis that was conducted using Fiji image analysis software to quantify the percentage of bone surface area stained by TRAP and Von Kossa are indicated at the right of the images (n = 4). One-way ANOVA followed by a Dunn's multiple comparison for multiple groups was used. Data are presented as mean ± SEM. Source data are provided in Supplementary Data.

soluble, catalytically active conformation in the tetramer. PDI also uses its KDEL motif to retain the C-P4H tetramer in the ER lumen.

Osteoblasts and adipocytes are both differentiated from MSCs and share a common precursor, exhibiting plasticity between these cell types. In this study, femora from Osx-Cre/PDI$^{fl/wt}$ mice showed an increase in the number of adipocytes and a decrease in osteoblasts in the femora compared with those from control mice, suggesting that PDI promotes the MSCs differentiation into osteoblasts and suppresses their differentiation into adipocytes. The differentiation of adipocytes is primarily regulated by two transcription factors, C/EBPα and PPARγ. PDI deletion increased the expression of C/EBPα and PPARγ (Fig. 4), indicating that PDI regulates the differentiation of MSCs into adipocytes via the modulation of C/EBPα and PPARγ expression[32,33]. Numerous in vitro studies have shown that adipokines inhibit osteogenesis and, conversely, that osteoinductive factors impede adipogenesis. The regulatory mechanism of PDI in the direction of MSCs differentiation awaits further investigation.

Previous studies have demonstrated that PDI inhibitors can reduce osteoclast numbers and inhibit their resorption function by suppressing the expression of osteoclast marker genes[34]. In consistent, our results indicated that PDI deficiency decreased osteoclast numbers. Osteoblasts regulate

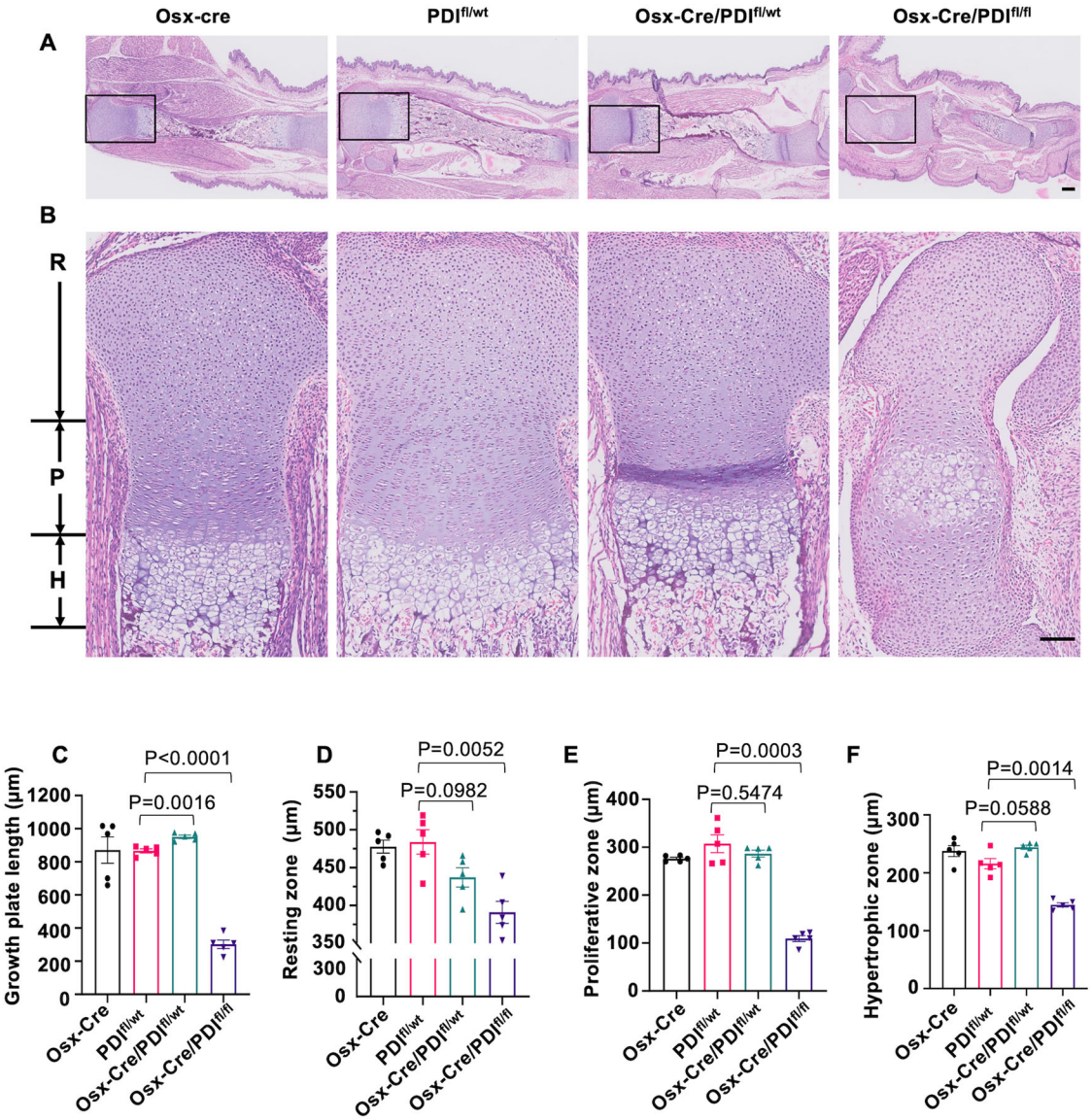

Fig. 6 | Comparison of tibia growth plate length, resting zone, proliferative and hypertrophic zone. A Tibias from Osx-Cre/PDI$^{fl/wt}$ and Osx-Cre/PDI$^{fl/fl}$ mice, as well as those from Osx-Cre and PDI$^{fl/wt}$ mice at E18.5, were processed for histological analysis and stained with hematoxylin and eosin (H&E) to assess tissue morphology. Scale bars = 200 μm. **B** Higher magnification images of the growth plate were obtained, highlighting the resting (R), proliferative (P), and hypertrophic (H) zones for detailed examination. Scale bars = 100 μm. Quantification of the total growth plate (**C**), resting zone (**D**), proliferative zone (**E**) and hypertrophic zone (**F**) was conducted based on the images in (**B**). n = 5 in each group. One-way ANOVA followed by a Dunn's multiple comparison for multiple groups was used. Data are presented as mean ± SEM. Source data are provided in Supplementary Data.

osteoclast activity by secreting OPG and RANKL. This regulatory mechanism involves signaling and receptor-ligand interactions between cells[35,36]. OPG functions as a pseudoreceptor for RANKL, and by binding to it, prevents RANKL from binding to RANK receptors on the surface of osteoclast precursor cells. In the absence of PDI, the secretion of OPG by osteoblasts was up-regulated, whereas the level of RANKL remained unchanged (Fig. 7E), which perhaps caused a decrease in the number and activation of osteoclasts.

Taken together, this study demonstrates the essential role of PDI in osteoblast function and differentiation, as well as bone development, which is closely associated with collagen synthesis and the regulation of the differentiation of osteoblasts and adipocytes. The identification of the critical role of PDI in bone biology reveals that the dysfunctional PDI is a novel pathogenesis of osteogenesis imperfecta and osteoporosis. PDI could be a new target for gene therapy of these disorders.

Materials and methods

Mouse strains

The PDI$^{fl/fl}$ mice were generated by the International Knockout Mouse Consortium (IKMC) at the Cambridge-Suda Genomic Resource Center. This was accomplished using embryonic stem cells harboring a floxed PDI gene (clone number: EPD0317_6_D10). The targeting vector included loxP sites positioned between exons 2 and 3, and between the fourth loxP site and exon 5 of the PDI gene. This vector was subsequently introduced into fertilized mouse oocytes to facilitate endogenous integration. The recombination between the two FRT sites was achieved by expression of Flp recombinase under the control of the β-actin promoter. For osteoblast-specific PDI gene knockout, PDI$^{fl/fl}$ mice were crossed with Osx-Cre transgenic mice obtained from The Jackson Laboratory. This mating strategy facilitated the excision of exons 3 and 4 by recombination between the two loxP sites, thereby resulting in the deletion of the PDI gene.

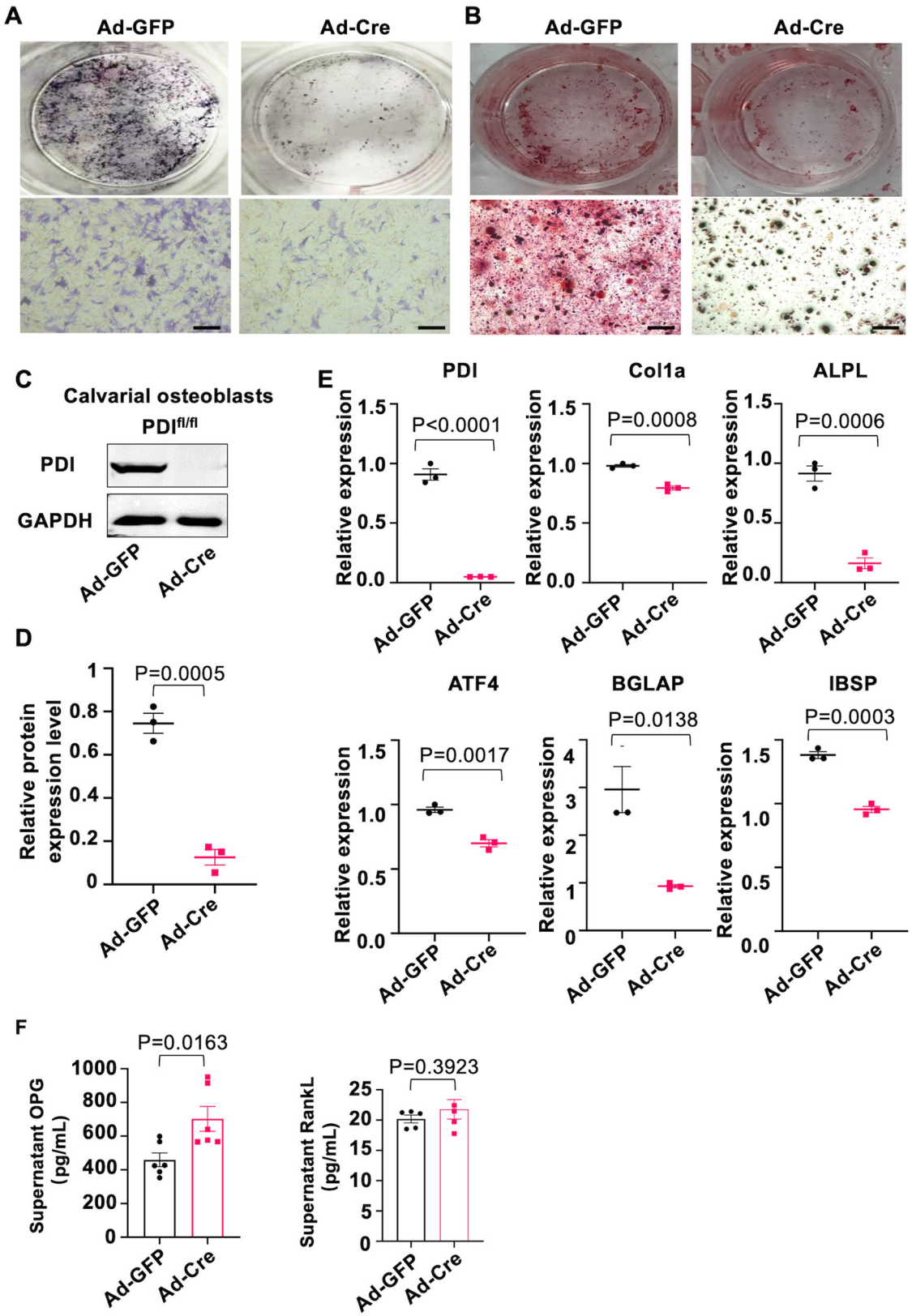

All experiments involving mice were conducted in strict accordance with the institutional guidelines and were approved by the Institutional Animal Care and Use Committee of Soochow University. The overall development and health of the animals were monitored following the guidelines set forth by the Association for Assessment and Accreditation of Laboratory Animal Care (AAALAC). Mice were housed in a specific pathogen-free (SPF) facility at Soochow University, maintained on a 12-h light/dark cycle, with temperature controlled at 24 ± 2°C and humidity maintained at 55 ± 5%. Both male and female mice and embryos were used.

Fig. 7 | PDI deficiency inhibits osteoblast function and differentiation. Primary osteoblast precursors were isolated from the calvarium of neonatal PDI$^{fl/fl}$ mice. These cells were subsequently infected with adenoviruses encoding GFP (Ad-GFP) or Cre recombinase (Ad-Cre) to induce PDI gene deletion. **A** Alizarin Red S staining of wild-type (Ad-GFP) versus PDI deficient (Ad-Cre) calvarial cells after 14 days of osteogenic differentiation. Scale bars = 40 μm. **B** Alkaline phosphatase (ALP) staining of wild-type (Ad-GFP) versus PDI-deficient (Ad-Cre) calvarial cells after 7 days of osteogenic differentiation. **C** Western blot of PDI protein. PDI protein in whole-cell lysates from PDI$^{fl/fl}$ primary osteoblasts was diminished 48 h after Ad-Cre infection (PDI) compared with Ad-GFP infection (control). The original blots are shown in Supplementary file as Supplementary Fig. 3. **D** Quantification of PDI protein expression levels relative to GAPDH using grayscale value analysis performed by ImageJ, showing a significant reduction in PDI expression in Ad-Cre-infected cells compared to Ad-GFP-infected cells (n = 3). **E** Calvarial osteoblasts were cultured in osteogenic medium for 7 days following infection with Ad-GFP or Ad-Cre. Total RNA was extracted, and the expression levels of osteoblast differentiation markers (Col1a, ALPL, ATF4, BGLAP, and IBSP) were quantified using qPCR (n = 3). **F** OPG and RANKL levels were measured in the culture supernatant of primary Ad-Cre- and Ad-GFP-infected osteoblasts after induction of differentiation for 7 days (n = 4–6 per group). Two-tailed Student's t test were used. Data are presented as mean ± SEM. Source data are provided in Supplementary Data.

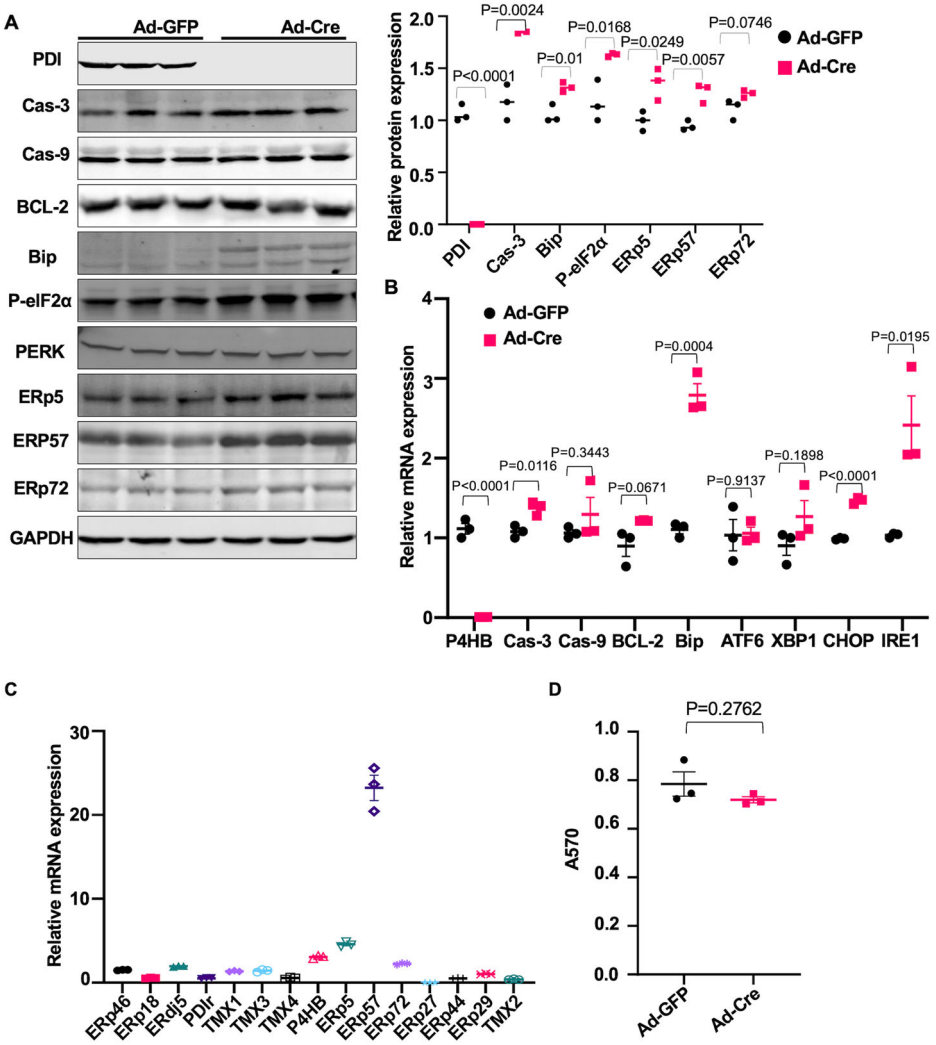

Fig. 8 | Loss of PDI in osteoblasts triggers apoptosis and ER stress. A Western blot analysis was performed to assess ER stress and apoptotic markers in wild-type (Ad-GFP) and PDI-deficient (Ad-Cre) calvarial cells after 7 days of osteogenic differentiation or 3 days of culture. GAPDH was considered as the internal reference (n = 3). The original blots are shown in Supplementary file as Supplementary Fig. 4.**B** Quantification of the relative protein expression levels was performed using grayscale analysis in ImageJ, normalized to GAPDH. Significant differences between Ad-GFP and Ad-Cre groups were indicated (n = 3). **C** qPCR analyses of osteoblast ER stress and apoptotic markers in wildtype (Ad-GFP) versus PDI-deficient (Ad-Cre) calvarial cells (n = 3). **D** The abundance of mRNA levels of PDI family genes, which encodes protein disulfide isomerase, were analyzed by qPCR. **E** Primary calvarial cells isolated from PDI$^{fl/fl}$ neonates and infected with adenoviruses expressing GFP (Ad-GFP) or Cre (Ad-Cre) for 3 days, and cell viability was examined by MTT assay (n = 3). Two-tailed Student's t test were used. Data are presented as mean ± SEM. Source data are provided in Supplementary Data.

Histological analysis

Isolated tissues were fixed in 4% paraformaldehyde in PBS overnight. Bones were decalcified in 14% EDTA/PBS for two weeks. Decalcified bones were dehydrated and embedded in paraffin or OCT. The sections were stained with hematoxylin and eosin (H&E), tartrate resistant acid phosphatase (TRAP), Oil Red O. As for von Kossa staining, no decalcification was required.

Picrosirius red staining and quantification

The femur was isolated and decalcified in 14% EDTA. After embedding in paraffin, 4 μm thick sections were generated and stained for 1 h, according to the manufacturer's instructions. Adobe Photoshop software was used to delimit the region of interest (ROI), the quantification of the intensity of birefringence brightness (pixels^2) was performed using the Fiji software to define total area of green, yellow, and red collagen fibers.

Whole-mount skeletal staining

Embryonic mice at 18.5 days were washed in PBS and then blanched in tap water at 65 °C for 20–30 s to promote tissue maceration and skin removal. For skeletal preparation, mice were skinned, eviscerated, and fixed in 95% ethanol before staining with Alcian blue and Alizarin red solutions. This was followed by tissue clarification with KOH. Finally, cartilage and bone mineralization were then characterized by different colors (blue and red, respectively)[37].

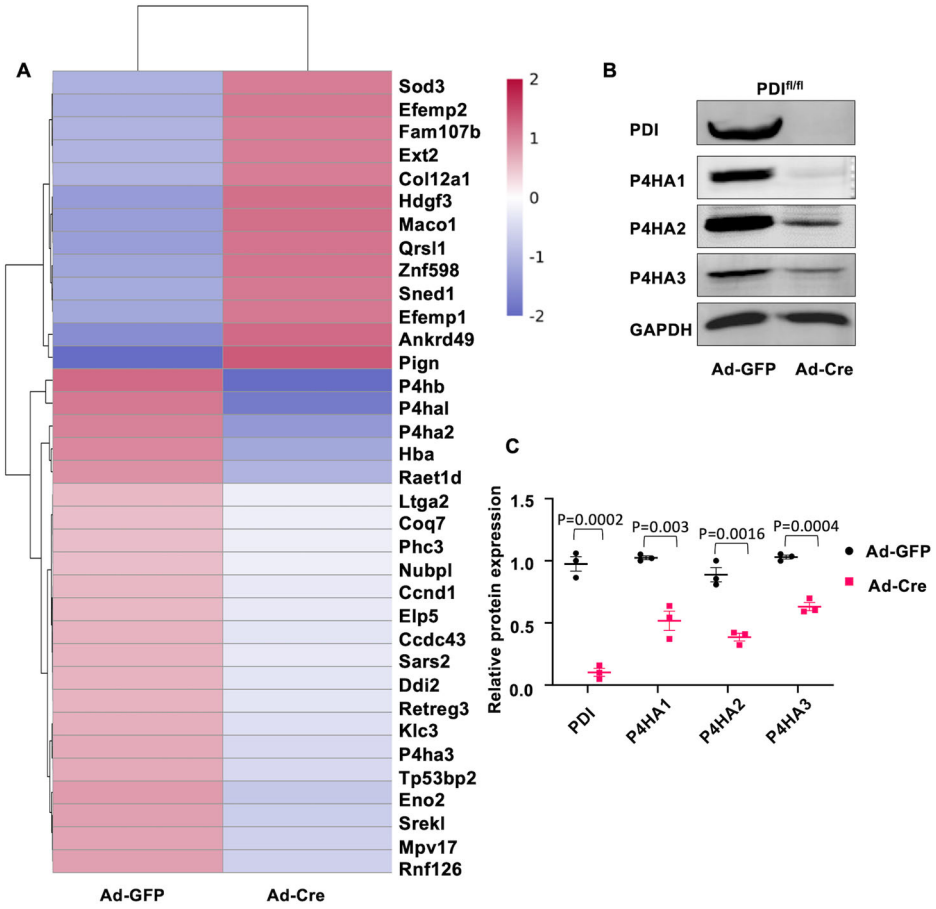

Fig. 9 | Prolyl hydroxylase α subunits are major substrates of PDI in osteoblasts. A Proteomic analysis via LC-MS/MS comparing wild-type (Ad-GFP) and PDI-deficient (Ad-Cre) calvarial osteoblasts isolated from PDIfl/fl mice, differentiated for 7 days post-infection. The heat map illustrates differentially expressed proteins (upregulated in red, downregulated in purple), revealing distinct clustering patterns between the groups. **B** Western blot analysis of lysates from osteoblasts differentiated for 7 days following Ad-GFP or Ad-Cre infection to assess the protein levels of PDI, P4HA1, P4HA2, and P4HA3. GAPDH was used as a loading control. The original blots are shown in Supplementary file as Supplementary Fig. 5. **C** Semiquantitative analysis of Western blot bands was performed using ImageJ to quantify the relative expression levels of PDI, P4HA1, P4HA2, and P4HA3, normalized to GAPDH (n = 3). Two-tailed Student's t test were used. Data are presented as mean ± SEM. Source data are provided in Supplementary Data.

Micro-CT

Femurs were fixed in 4% paraformaldehyde, washed, and transferred to 70% ethanol. Specimens were scanned using Bruker Micro-CT Skyscan 1276 system (Kontich, Belgium). Scan settings are as follows: voxel size 6.534165 µm, medium resolution, 70 kV, 200 uA,0.25 mm Al filter and integration time 350 ms. Reconstruction was accomplished by NRecon (version 1.7.4.2). 3D images were obtained from contoured 2D images by methods based on distance transformation of the grayscale original images (CTvox; version 3.3.0). 3D and 2D analysis were performed using software CT Analyser (version 1.20.3.0).

Calcein labeling assay

Calcein solution in saline (1 mg/mL) was administered to 3-week-old mice via intraperitoneal injection (i.p.) at a dose of 10 mg/kg body weight, with a second injection performed four days after the initial administration. Following the final injection, the femurs were collected, fixed in 4% paraformaldehyde, and subsequently dehydrated through a graded series of ethanol concentrations (75–100%). The dehydrated samples were then embedded in methyl methacrylate to facilitate sectioning. Serial midsagittal sections with a thickness of 100 µm were obtained for histological analysis. The fluorescent signals corresponding to calcein labeling within the cortical bone were visualized using an Olympus fluorescence microscope. The distance between the two calcein-labeled lines, which represented the newly mineralized bone between the two injection time points, was measured using ImageJ software. These measurements were utilized to calculate the mineral apposition rate (MAR), providing a quantitative assessment of the bone formation rate.

Primary calvarial cell isolation and adenovirus infection

To isolate calvarial cells, newborn $PDI^{fl/fl}$ pups were euthanized by decapitation using sharp scissors. Subsequently, the frontal and parietal bones were dissected, rinsed with PBS. The calvariae were transferred into a 50 mL conical tube and digested in 1 mg·mL−1 collagenase A (Roche) in serum-free αMEM in a 37 °C water bath for 15 min. The first digestion was discarded while digestions two to five were combined and filtered through a 70 µm cell strainer. Cells were seeded in 12-well plate sat 1.5×10^5 cells/well and cultured overnight. Cells were infected with adenovirus expressing either green fluorescence protein (Ad-GFP) or Cre (Ad-CRE) at a multiplicity of infection of 50. At 72 h after adenoviral infection, cells were either harvested for protein analysis or induced for osteoblast differentiation by osteogenic medium (αMEM media with 10% FBS, 10 mM β-glycerol phosphate and 50 µg/ml ascorbic acid). Osteogenic medium was changed every other day.

Alkaline phosphatase staining and Alizarin Red S staining

For ALP staining, cells were fixed with 4% formaldehyde, rinsed with PBS, and then incubated with 1-Step NBT/BCIP (Sigma) at room temperature for 20 minutes. For Alizarin Red S staining, cells were fixed with 4% paraformaldehyde for 30 min and removed. Next, 500 µl Alizarin red S staining solution (Sigma) was added to cover the cell surface and was incubate at room temperature in the dark for 20 min. Excess stain was washed off with double distilled water.

Protein identification and quantification by LC-MS/MS

Calvarial osteoblasts from $PDI^{fl/fl}$ mice were differentiated for 7 days post-infection with Ad-Cre and Ad-GFP. Samples were lysed in buffer (8 M urea, 1% protease inhibitor) via ultrasonication, centrifuged at 12,000 × *g* for 10 min at 4 °C, and the supernatant was used for protein quantification (BCA assay). Equal protein amounts were digested after volume normalization. Precipitation was induced with 20% TCA at 4 °C for 2 h, followed by centrifugation at 4500 × *g* for 5 min. The resulting pellets were washed with pre-cooled acetone, air-dried, resuspended in 200 mM TEAB, and subjected to overnight trypsin digestion (1:50 enzyme-to-protein ratio). Peptides were reduced with 5 mM

DTT at 56°C for 30 minutes and alkylated with 11 mM IAA in the dark at room temperature for 15 minutes. Peptides were then separated using the NanoElute UHPLC system with a gradient of 7–24% B (0–72 min), 24–32% B (72–84 min), 32–80% B (84–87 min), and 80% B (87–90 min) at 450 nL/min. Peptide analysis was conducted on a timsTOF Pro mass spectrometer in PASEF mode, with a scan range of 100–1700 m/z and a dynamic exclusion time of 30 seconds. The results were visualized using a heatmap, where protein expression levels were compared between Ad-GFP and Ad-Cre infected cells, highlighting the differential expression of various proteins.

Quantitative real-time PCR (qPCR) and Western blot

Total RNA was extracted from primary calvarial osteoblasts using a FreeZol Reagent (Vazyme). Reverse transcription was performed with HiScript IV All-in-One Ultra RT SuperMix for qPCR kit (Vazyme). All real-time PCR reactions were performed using a 7500 Real-time PCR System (Applied Biosystems) and the Taq Pro Universal SYBR qPCR Master Mix Kit (Vazyme). The relative quantification of gene expression was calculated using the ΔΔCt method. Relative gene expression was determined by first normalization to β-actin, and then normalization to control samples. (primer names and sequences are listed as supplementary Table 1 in supplementary files). Western blot analysis was performed on lysates from cultured primary osteoblasts. The cell lysates were separated by sodium dodecyl sulfate–polyacrylamide gel electrophoresis (SDS-PAGE) using electrophoresis, and then the proteins were transferred to polyvinylidene difluoride (PVDF) membrane. After being blocked with 5% non-fat milk or BSA for 1 h, the membranes were incubated with primary anti-PDI, ERp5, ERP72 (ABclonal), P4HA1, P4HA2, P4HA3, (ProteinTech), Caspase 3, Caspase 9, Bcl-2, Bip PERK (Abmart), p-elF2α and GAPDH (Cell Signaling Technology) at 4 °C overnight. All antibodies were used at a ratio of 1:1000. After being washed three times with TBST, the membranes were incubated with an appropriate secondary antibody (LI-COR Bioscience). Finally, the membranes were determined by ODYSSEY infrared imaging system (LI-COR) and were quantified by the ImageJ software.

Enzyme-linked immunosorbent assay (ELISA)

Serum samples were collected from mouse whole blood by centrifugation for 20 min at approximately 1000 × *g*. We used the RANKL (TNFSF11) Mouse ELISA Kit to measure levels of RANKL in osteoblast cultures according to the manufacturer's instructions.

Osteoblast proliferation assay

After exposure to adenovirus, the osteoblasts were plated on 96-well plates (at 1×10^4 cells/well). Cell proliferation assay was determined using the MTT Cell Proliferation and Cytotoxicity Assay Kit (Beyotime) according to the manufacturer's instructions. MTT was dissolved in PBS at a concentration of 5 mg/ml and sterilized by passage through a 0.22-μm filter. This stock solution (10 μl) was added to each well, and the plate was incubated at 37 °C for 4 h. Formazan was added to all wells and mixed thoroughly to dissolve the dark blue crystals. After 3–4 h at room temperature, to ensure that all the crystals were dissolved, the plates were read on a microplate reader at a wavelength of 570 nm.

Statistics and reproducibility

At least triplicate experiments were included for statistical analysis. The sample size for each experiment is provided within the respective figure legends. Data analysis was performed using the GraphPad Prism8 software. Two-tailed *t* test for two groups and One-way ANOVA followed by a Dunn's multiple comparison for multiple groups and were used. Quantitative data was expressed as the Mean ± SEM. $p < 0.05$ was considered statistically significant.

Reporting summary

Further information on research design is available in the Nature Portfolio Reporting Summary linked to this article.

Data availability

The data of mass spectrometry generated in this study have been deposited in ProteomeXchange with identifier PXD 060949. Uncropped and unedited blot images (Supplementary Figs. 3–5) and other data have been included in the Supplementary file. All other data are available from the corresponding author on reasonable request.

Received: 19 January 2024; Accepted: 26 February 2025;
Published online: 10 March 2025

References

1. Ferrari, D. M. & Soling, H. D. The protein disulphide-isomerase family: unravelling a string of folds. *Biochem. J.* **339**, 1–10 (1999).
2. Galligan, J. J. & Petersen, D. R. The human protein disulfide isomerase gene family. *Hum Genomics* **6**, 6 (2012).
3. Freedman, R. B., Hirst, T. R. & Tuite, M. F. Protein disulfide-isomerase - building bridges in protein-folding. *Trends Biochem. Sci.* **19**, 331–336 (1994).
4. Freedman, R. B., Klappa, P. & Ruddock, L. W. Protein disulfide isomerases exploit synergy between catalytic and specific binding domains. *EMBO Rep.* **3**, 136–140 (2002).
5. Wilkinson, B. & Gilbert, H. F. Protein disulfide isomerase. *Bba-Proteins Proteom.* **1699**, 35–44 (2004).
6. Pihlajaniemi, T. et al. Molecular-cloning of the beta-subunit of human prolyl 4-hydroxylase - this subunit and protein disulfide isomerase are products of the same gene. *EMBO J.* **6**, 643–649 (1987).
7. Wetterau, J. R., Combs, K. A., Spinner, S. N. & Joiner, B. J. Protein disulfide isomerase is a component of the microsomal triglyceride transfer protein complex. *J. Biol. Chem.* **265**, 9800–9807 (1990).
8. Montane, J. et al. Protein disulfide isomerase ameliorates beta-cell dysfunction in pancreatic islets overexpressing human islet amyloid polypeptide. *Mol. Cell Endocrinol.* **420**, 57–65 (2016).
9. Khan, H. A. & Mutus, B. Protein disulfide isomerase a multifunctional protein with multiple physiological roles. *Front. Chem.* **2**, 70 (2014).
10. Xu, S. L., Sankar, S. & Neamati, N. Protein disulfide isomerase: a promising target for cancer therapy. *Drug Discov. Today* **19**, 222–240 (2014).
11. Andreu, C. I., Woehlbier, U., Torres, M. & Hetz, C. Protein disulfide isomerases in neurodegeneration: From disease mechanisms to biomedical applications. *FEBS Lett.* **586**, 2826–2834 (2012).
12. Wang, Y. et al. Impaired bone formation in deficient mice. *Plos One* **9**, e112708 (2014).
13. Rauch, F. et al. Cole-carpenter syndrome is caused by a heterozygous missense mutation in P4HB. *Am. J. Hum. Genet* **96**, 425–431 (2015).
14. Cole, D. E. C. & Carpenter, T. O. Bone fragility, craniosynostosis, ocular proptosis, hydrocephalus, and distinctive facial features - a newly recognized type of osteogenesis imperfecta. *J. Pediatr.-US* **110**, 76–80 (1987).
15. Rauch, F. & Glorieux, F. H. Osteogenesis imperfecta. *Lancet* **363**, 1377–1385 (2004).
16. Van Dijk, F. S. & Sillence, D. O. Osteogenesis imperfecta: Clinical diagnosis, nomenclature and severity assessment. *Am. J. Med. Genet A* **164**, 1470–1481 (2014).
17. Deng, F. Y. et al. Proteomic analysis of circulating monocytes in Chinese premenopausal females with extremely discordant bone mineral density. *Proteomics* **8**, 4259–4272 (2008).
18. Balasubramanian, M. et al. P4HB recurrent missense mutation causing Cole-Carpenter syndrome. *J. Med. Genet* **55**, 158–165 (2018).
19. Li, L. J. et al. A novel missense mutation in P4HB causes mild osteogenesis imperfecta. *Biosci. Rep.* **39**, BSR20182118 (2019).
20. Porntaveetus, T., Theerapanon, T., Srichomthong, C. & Shotelersuk, V. Cole-Carpenter syndrome in a patient from Thailand. *Am. J. Med. Genet A* **176**, 1706–1710 (2018).

21. Ouyang, L. X. & Yang, F. Cole-Carpenter syndrome-1 with a de novo heterozygous deletion in the P4HB gene in a Chinese girl: A case report. *Medicine* **96**, e9504 (2017).
22. Cao, Y. J., Zhang, H. & Zhang, Z. L. Novel Mutations in the Wnt1, Tmem38b, P4hb, and Pls3 genes in four unrelated Chinese families with osteogenesis imperfecta. *Endocr. Pract.* **25**, 230–241 (2019).
23. Cotrina-Vinagre, F. J. et al. Characterization of a complex phenotype (fever-dependent recurrent acute liver failure and osteogenesis imperfecta) due to NBAS and P4HB variants. *Mol. Genet Metab.* **133**, 201–210 (2021).
24. Zhou, J. et al. The C-terminal CGHC motif of protein disulfide isomerase supports thrombosis. *J. Clin. Invest* **125**, 4391–4406 (2015).
25. Willett, T. L., Dapaah, D. Y., Uppuganti, S., Granke, M. & Nyman, J. S. Bone collagen network integrity and transverse fracture toughness of human cortical bone. *Bone* **120**, 187–193 (2019).
26. Vuori, K., Myllyla, R., Pihlajaniemi, T. & Kivirikko, K. I. Expression and site-directed mutagenesis of human protein disulfide isomerase in Escherichia coli. This multifunctional polypeptide has two independently acting catalytic sites for the isomerase activity. *J. Biol. Chem.* **267**, 7211–7214 (1992).
27. Canalis, E. Notch Signaling in Osteoblasts. *Sci. Signal* **1**, pe17 (2008).
28. Jensen, E. D., Gopalakrishnan, R. & Westendorf, J. J. Regulation of gene expression in osteoblasts. *Biofactors* **36**, 25–32 (2010).
29. Collins, F. L., Rios-Arce, N. D., Schepper, J. D., Parameswaran, N. & McCabe, L. R. The potential of probiotics as a therapy for osteoporosis. *Microbiol Spectr.* **5** 1–16 (2017).
30. McCarthy, T. L. & Centrella, M. Prostaglandin dependent control of an endogenous estrogen receptor agonist by osteoblasts. *J. Cell Physiol.* **230**, 1104–1114 (2015).
31. Serrano, A. et al. Reversal of alpha-synuclein fibrillization by protein disulfide isomerase. *Front Cell Dev. Biol.* **8**, 726 (2020).
32. Rosen, E. D. & MacDougald, O. A. Adipocyte differentiation from the inside out. *Nat. Rev. Mol. Cell Biol*. **7**, 885–896 (2006).
33. Caplan, A. I. & Bruder, S. P. Mesenchymal stem cells: Building blocks for molecular medicine in the 21st century. *Trends Mol. Med.* **7**, 259–264 (2001).
34. Wang, Y. et al. Inhibition of protein disulfide isomerase attenuates osteoclast differentiation and function via the readjustment of cellular redox state in postmenopausal osteoporosis. *Inflammation* **47**, 626–648 (2024).
35. Lacey, D. L. et al. Osteoprotegerin ligand is a cytokine that regulates osteoclast differentiation and activation. *Cell* **93**, 165–176 (1998).
36. Sims, N. A. & Gooi, J. H. Bone remodeling: Multiple cellular interactions required for coupling of bone formation and resorption. *Semin Cell Dev. Biol.* **19**, 444–451 (2008).
37. Rigueur, D. & Lyons, K. M. Whole-mount skeletal staining. *Methods Mol. Biol.* **1130**, 113–121 (2014).

Acknowledgements

This work was supported by grants from the National Natural Science Foundation of China (81970128, 82270136, 82170129, 82470132, 31970890, 8217011021, 82020108003), the Translational Research Grant of NCRCH (2020ZKPA02, 2020WSA04), the Jiangsu Provincial Medical Innovation Center (CXZX202201), the collaboration fund from State Key Laboratory of Radiation Medicine and Protection (GZN1201802), the Priority Academic Program Development of Jiangsu Higher Education Institutions.

Author contributions

Y.L., A.Y, and Z.Z. performed the experiments, Y.H. assisted with experimental performance and critical reagents. Y.L., D.W. and Y.W. conceived and designed the study, and wrote the manuscript.

Competing interests

The authors declare no competing interests.

Additional information

Supplementary information The online version contains supplementary material available at https://doi.org/10.1038/s42003-025-07824-3.

Correspondence and requests for materials should be addressed to Yue Lu, Depei Wu or Yi Wu.

Peer review information *Communications Biology* thanks Fayez Safadi and the other, anonymous, reviewer for their contribution to the peer review of this work. Primary Handling Editor: Dario Ummarino.

Reprints and permissions information is available at http://www.nature.com/reprints

Publisher's note Springer Nature remains neutral with regard to jurisdictional claims in published maps and institutional affiliations.

Open Access This article is licensed under a Creative Commons Attribution-NonCommercial-NoDerivatives 4.0 International License, which permits any non-commercial use, sharing, distribution and reproduction in any medium or format, as long as you give appropriate credit to the original author(s) and the source, provide a link to the Creative Commons licence, and indicate if you modified the licensed material. You do not have permission under this licence to share adapted material derived from this article or parts of it. The images or other third party material in this article are included in the article's Creative Commons licence, unless indicated otherwise in a credit line to the material. If material is not included in the article's Creative Commons licence and your intended use is not permitted by statutory regulation or exceeds the permitted use, you will need to obtain permission directly from the copyright holder. To view a copy of this licence, visit http://creativecommons.org/licenses/by-nc-nd/4.0/.

© The Author(s) 2025